8766 *Biochemistry* **2010,** *49,* 8766–8778
DOI: 10.1021/bi101050h

BIOCHEMISTRY
including biophysical chemistry & molecular biology
Article

A Biosensor Study Indicating That Entropy, Electrostatics, and Receptor Glycosylation Drive the Binding Interaction between Interleukin-7 and Its Receptor[†]

Scott T. R. Walsh*

Department of Cell Biology and Molecular Genetics, Institute for Bioscience and Biotechnology Research, W. M. Keck Laboratory for Structural Biology, University of Maryland, 9600 Gudelsky Drive, Rockville, Maryland 20850

Received July 1, 2010; Revised Manuscript Received September 2, 2010

ABSTRACT: The interaction between interleukin-7 (IL-7) and its α-receptor, IL-7Rα, plays fundamental roles in the development, survival, and homeostasis of B- and T-cells. N-Linked glycosylation of human IL-7Rα enhances its binding affinity for human IL-7 300-fold versus that of the nonglycosylated receptor through an allosteric mechanism. The N-glycans of IL-7Rα do not participate directly in the binding interface with IL-7. This biophysical study involves dissection of the properties of binding of IL-7 to both nonglycosylated and glycosylated forms of the IL-7Rα extracellular domain (ECD) as functions of salt, pH, and temperature using surface plasmon resonance (SPR) spectroscopy. Interactions of IL-7 with both IL-7Rα variants display weaker binding affinities with increasing salt concentrations primarily reflected by changes in the first on rates of a two-step reaction pathway. The electrostatic parameter of the IL-7−IL-7Rα interaction is not driven by complementary charge interactions through residues at the binding interface or N-glycan composition of IL-7Rα, but presumably by favorable global charges of the two proteins. van't Hoff analysis indicates both IL-7−IL-7Rα interactions are driven by large favorable entropy changes and smaller unfavorable (nonglycosylated complex) and favorable (glycosylated complex) enthalpy changes. Eyring analysis of the IL-7−IL-7Rα interactions reveals different reaction pathways and barriers for the transition-state thermodynamics with the enthalpy and entropy changes of IL-7 binding to nonglycosylated and glycosylated IL-7Rα. There were no discernible heat capacity changes for the equilibrium or transition-state binding thermodynamics of the IL-7−IL-7Rα interactions. The results suggest that the unbound nonglycosylated IL-7Rα samples an extensive conformational landscape relative to the unbound glycosylated IL-7Rα, potentially explaining the switch from a "conformationally controlled" reaction ($k_1 \sim 10^2$ M^{-1} s^{-1}) for the nonglycosylated interaction to a "diffusion-controlled" reaction ($k_1 \sim 10^6$ M^{-1} s^{-1}) for the glycosylated interaction. Thus, a large favorable entropy change, a global favorable electrostatic component, and glycosylation of the receptor, albeit not at the interface, contribute significantly to the interaction between IL-7 and the IL-7Rα ECD.

The development, proliferation, and homeostasis of immune cells are orchestrated through numerous signaling pathways. At the heart of these signaling pathways are the interactions of soluble cytokines with membrane-bound cytokine receptors on cellular surfaces. The external stimulus of a cytokine binding a cytokine receptor is relayed across the cell membrane to intracellular events ultimately altering the behavior of the targeted cell. While these binding events between cytokines and cytokine receptors are conceptually straightforward, the structural and molecular recognition principles underlying these interactions are complex and unpredictable. A further layer of complexity of the cytokine−cytokine receptor field involves pleiotropy, in which cytokines or receptors are programmed to bind and function through multiple ligands.

The interleukin-7 (IL-7)[1] signaling pathway is one of these critical cascades of the immune system. The IL-7 signaling pathway is triggered when IL-7 binds to the extracellular domains (ECDs) of its own specific α-receptor, IL-7Rα (CD127), and the common γ-chain receptor, γ_c (CD132) (reviewed in refs *1* and *2*). The attraction of the two cytokine receptors by IL-7 activates kinases on the intracellular domains of the receptors to phosphorylate themselves and other sequence elements, leading to subsequent recruitment of transcription factors. Once the transcription factors interact with the intracellular domains of the cytokine receptors, the kinases phosphorylate the transcription factors, which subsequently dissociate from the cytokine receptor, oligomerize, and localize to the nucleus to elevate transcription and the cellular response (reviewed in refs *1* and *2*). The IL-7 signaling pathway utilizes the JAK/Stat, PI3/Akt, and Src pathways to regulate cellular responses of immune cells (reviewed in refs *1* and *2*).

The IL-7 signaling pathway contributes to early and late events during the immunological response. The IL-7 pathway is fundamental to the development of B-cell pools in mice and T-cell pools in mice and humans (reviewed in refs *1* and *2*). Mutations of the ECD of IL-7Rα lead to forms of severe combined immunodeficiencies

[†]This research was supported by grants from the American Heart Association (535131N) and National Institutes of Health (AI72142) to S.T.R.W.

*To whom correspondence should be addressed. Phone: (240) 314-6478. Fax: (240) 314-6225. E-mail: swalsh12@umd.edu.

[1]Abbreviations: SPR, surface plasmon resonance; IL-7, interleukin-7; IL-7Rα, interleukin-7 α-receptor; ECD, extracellular domain; CD, circular dichroism; GlcNAc, *N*-acetylglucosamine; MAN, mannose; $\Delta G°$, free energy change; $\Delta H°$, enthalpy change; $\Delta S°$, entropy change; pI, isoelectric point; PDB, Protein Data Bank.

 Published on Web 09/03/2010

(SCIDs) with the phenotype of T^- B^- NK^+ in mice and T^- B^+ NK^+ in humans (*3*). After development of B- or T-cells, expression of IL-7Rα is downregulated, and other γ_c family members play roles in the proliferation and differentiation of these immune cells (reviewed in ref *1*). After an immune response, IL-7Rα expression is upregulated and signaling occurs, which triggers anti-apoptotic factors of the *bcl2*/*mcl1* lineage to generate memory cells (reviewed in ref *1*). Another biological role of the IL-7 signaling pathway involves extracellular matrix remodeling (reviewed in ref *4*). IL-7Rα is a pleiotrophic cytokine receptor and functions in the thymic stromal lymphopoietin (TSLP) signaling pathway, thereby promoting activation of B-cells in mice and dendritic cells (DCs) in humans (*5*). The precise mechanisms of action of IL-7 and IL-7Rα are evolving.

IL-7 and IL-7Rα are both glycoproteins. No studies have reported any O-linked glycosylation sites of either IL-7 or IL-7Rα. While IL-7 comprises three potential N-linked glycosylation sites (N70, N91, and N116), glycosylation does not affect the binding of IL-7 to its receptors or its function (*6*). The same cannot be said of N-linked glycosylation of IL-7Rα. We have demonstrated that the IL-7Rα ECD uses N-linked glycosylation to modulate its binding properties with IL-7 (*7*). The functional relevance of IL-7Rα glycosylation is currently under investigation. There are six potential N-linked glycosylation sites of the IL-7Rα ECD: N29, N45, N131, N162, N212, and N213. All of these sites on the IL-7Rα ECD are glycosylated to varying degrees (unpublished results). The binding affinity of IL-7 for glycosylated IL-7Rα is enhanced 300-fold (K_d = 60 nM) versus its binding affinity for nonglycosylated IL-7Rα (K_d = 18 μM) (*7*). The 300-fold enhancement in the K_d of IL-7 for glycosylated IL-7Rα results primarily from a 5200-fold faster association rate (k_1 values of 1.1×10^6 and 2.1×10^2 M^{-1} s^{-1}, respectively) (*7*). The constants for binding of IL-7 to glycosylated IL-7Rα are not affected by carbohydrate composition, as demonstrated by similar binding constants for paucimannose hybrid (Schneider S2 insect cells) or complex (CHO cells) N-glycan structures (*7*). The most critical N-glycan components for the IL-7−IL-7Rα binding constants are the first *N*-acetylglucosamines (GlcNAcs) of the α-receptors' N-glycans (*7*).

We also reported previously the crystal structures of IL-7 bound to both nonglycosylated and glycosylated forms of the IL-7Rα ECD (*7*) (Figure 1). Comparison of the two complex structures revealed no large conformational changes induced by glycosylation of IL-7Rα. Surprisingly, the N-glycans of IL-7Rα do not participate directly within the IL-7−IL-7Rα binding interface. It was possible to visualize the first two GlcNAcs of the core N-glycans for N29, N45, and N131 of IL-7Rα. The closest N-glycan of N29 is > 10 Å from the closest atom of the interface. The other three N-glycans attached to N162, N212, and N213, although not observable in the electron density, are also distant from the IL-7−IL-7Rα interface. Thus, the contribution of glycosylation of IL-7Rα to the enhanced binding properties of IL-7 versus those of nonglycosylated IL-7Rα appears allosteric in nature.

Providing an improved understanding of the allosteric mechanism of IL-7Rα glycosylation, this work reports SPR binding studies for binding of IL-7 to both nonglycosylated and glycosylated IL-7Rα as functions of salt, pH, and temperature. The IL-7−IL-7Rα binding constants were probed by increasing sodium chloride concentrations to investigate the charge dependence and long-range electrostatic binding contributions. The effects of protonation on the binding constants were measured

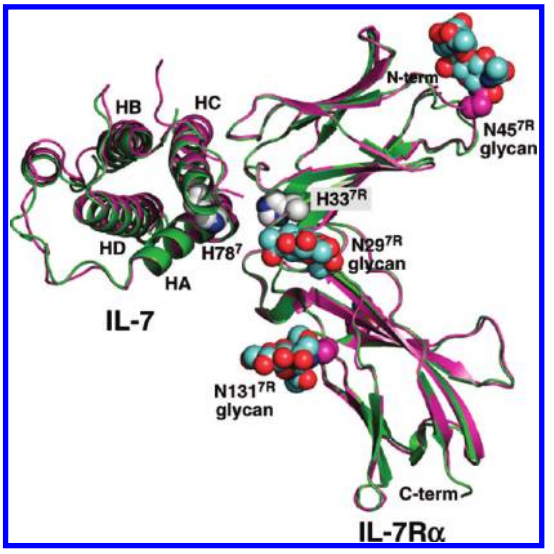

FIGURE 1: Ribbon diagrams of the complex structures of IL-7 bound to nonglycosylated (green, PDB entry 3di2) and glycosylated (magenta, PDB entry 3di3) forms of IL-7Rα (*7*). The nonglycosylated complex was superimposed onto the glycosylated complex. The four-α-helix bundle of IL-7 is labeled helix A (HA), helix B (HB), helix C (HC), and helix D (HD) accordingly. The N-glycans attached to $N29^{7R}$, $N45^{7R}$, and $N131^{7R}$ are colored as cyan CPK groups for the carbon atoms. The only histidine residues observed in the IL-7−IL-7Rα interface are $H78^7$ and $H33^{7R}$. The histidine side chains are drawn as white CPK groups for the carbon atoms. Oxygen and nitrogen atoms are colored red and blue, respectively. This figure was created and rendered using PyMOL (*58*).

with an increase in pH to investigate the two histidine residues in the binding interface (Figure 1, one from IL-7, $H78^7$, where the superscript 7 denotes IL-7 residues, and one from IL-7Rα, $H33^{7R}$, where the superscript 7R denotes IL-7Rα residues). Temperature studies of the binding affinities using van't Hoff analysis provided a breakdown of the binding of IL-7 to both forms of IL-7Rα into the enthalpic and entropic components of the free energy changes. Temperature studies of the binding kinetics using Eyring analysis of IL-7 and IL-7Rα (EC = *Escherichia coli* for the nonglycosylated receptor, or CHO = for the glycosylated receptor) provided a quantitative analysis of the transition-state thermodynamics of the reaction pathways for binding of IL-7 to nonglycosylated and glycosylated IL-7Rα.

EXPERIMENTAL PROCEDURES

Protein Expression and Purification. The IL-7 proteins were expressed and purified from bacterial and S2 insect cells as described previously (*8*). The recombinant human IL-7Rα ECD from CHO cells was purchased from R&D Systems and used without further purification. The expression and purification of the wild-type human growth hormone receptor (hGHR) ECD from bacterial cells were performed as described previously (*9*, *10*).

SPR Data Analysis. Experiments were performed using a Biacore 3000 SPR instrument. The IL-7Rα ECD coupling and binding kinetics were measured using CM5 sensor chips. Detailed SPR coupling strategies using amine or thiol chemistries have been described previously (*7*). Similar binding kinetics were observed for the IL-7−IL-7Rα interactions using either amine- or thiol-coupled sensor chip surfaces (*7*).

Numerous SPR control experiments were performed for the interactions of IL-7 with both nonglycosylated and glycosylated IL-7Rα, and they indicate mass transport effects were negligible.

Nonspecific binding was not observed when IL-7 was injected over the underivatized flow cell. SPR experiments were conducted at a flow rate of 50 μL/min and involved 2-fold serial dilutions of five IL-7 concentrations determined by the binding affinity for the IL-7Rα ECD. Each 250 μL protein or buffer injection was followed by a 400 s dissociation period. The surfaces were regenerated for subsequent runs with a 5 μL injection of 4 M $MgCl_2$. The running buffer consisted of 10 mM HEPES (pH 7.4), 150 mM NaCl, 3 mM EDTA, and 0.005% Tween 20 for the temperature dependence experiments. The same buffer was used for the ionic strength dependence experiments, with the exception of varying NaCl concentrations. For the pH experiments, either 10 mM sodium acetate (pH 5.5), 10 mM MES (pH 6.0−6.5), or 10 mM HEPES (pH 7.0−8.0) was used as the buffering chemical supplemented with 150 mM NaCl, 3 mM EDTA, and 0.005% Tween 20. The salt and pH binding experiments were performed at 298 K.

Sensorgrams were trimmed and double-referenced (*11*) using BIAevaluation version 4.1 before data analysis. The interaction of IL-7 with IL-7Rα-coupled surfaces fit best to a two-step (three-state) reaction model (*7*) originally described for SPR analysis by (*11*)

$$\text{IL-7} + \text{IL-7R}\alpha \underset{k_{-1}}{\overset{k_1}{\leftrightarrow}} [\text{IL-7}-\text{IL-7R}\alpha]^* \underset{k_{-2}}{\overset{k_2}{\leftrightarrow}} \text{IL-7}-\text{IL-7R}\alpha \quad (1)$$

Apparent equilibrium dissociation constants (K_d) were calculated using the following equation:

$$K_d = (k_{-1}k_{-2})/[k_1(k_2 + k_{-2})] \quad (2)$$

Sensorgrams were globally analyzed using ClampXP (*12*), and the binding kinetic parameters were determined from at least three separate experiments. Errors were propagated using Taylor series expansion described in detail in ref *13*.

Circular Dichroism. CD experiments were performed on an Aviv 62A DS spectropolarimeter (Aviv Biomedical, Inc.). The nonglycosylated and glycosylated IL-7Rα from *E. coli* and S2 insect cells and the hGHR ECD were buffer-exchanged into 10 mM sodium phosphate (pH 7.4) using a PD-10 desalting column (GE Healthcare). CD wavelength scans were recorded at 298 K from 186 to 280 nm with an 1 nm increment and a 20 s averaging period. The receptor protein concentrations were 16, 15, and 13.2 μM for IL-7Rα (EC), IL-7Rα (S2), and hGHR, respectively. The CD wavelength scans were recorded in 0.1 cm cells, and buffer wavelength scans were subtracted from the protein scans. Mean residue ellipticities were calculated using the relationship $[\theta] = \theta_{obs}/(10lcn)$, where θ_{obs} is the ellipticity measured in millidegrees, l is the path length of the cell in centimeters, c is the concentration in molar, and n is the number of protein residues.

RESULTS

NaCl Dependence of the IL-7−IL-7Rα Interactions. To assess the role of electrostatics in the IL-7−IL-7Rα binding interaction, the binding kinetics and affinities of IL-7 for nonglycosylated and glycosylated IL-7Rα were measured as a function of increasing NaCl concentrations using SPR spectroscopy. Assays were performed at sodium chloride concentrations of 50, 150, 300, 600, and 1000 mM at 298 K. For the IL-7−IL-7Rα (EC) interaction, reliable binding constants could be obtained up to a NaCl concentration of only 300 mM because the interaction of IL-7 with nonglycosylated IL-7Rα (EC) becomes too weak at higher concentrations. Binding constants were obtained over the entire NaCl concentration range for the IL-7−IL-7Rα (CHO) glycosylated interaction. The SPR sensorgrams from all experiments fit best to a two-step binding kinetic reaction model in which IL-7 and its receptor first form an "encounter complex" and second form the final IL-7−IL-7Rα complex. Figure 2 displays representative SPR sensorgrams (150 mM NaCl, pH 7.4, and 298 K) for the nonglycosylated and glycosylated IL-7−IL-7Rα binding interactions and global analysis curve fitting to one- and two-step binding reaction models. The binding constants are summarized in Tables S1 and S2 of the Supporting Information.

At 150 mM NaCl and 298 K, the nonglycosylated IL-7−IL-7Rα complex displays k_1, k_{-1}, k_2, and k_{-2} rates of $(3.26 \pm 0.82) \times 10^2$ M^{-1} s^{-1}, $(3.73 \pm 0.40) \times 10^{-2}$ s^{-1}, $(4.63 \pm 0.35) \times 10^{-3}$ s^{-1}, and $(1.44 \pm 0.084) \times 10^{-3}$ s^{-1}, respectively. The binding affinity (K_d) determined using eq 2 for this interaction is 27.1 ± 13 μM, which corresponds to a free energy change ($\Delta G°$) of −6.2 ± 0.2 kcal/mol. The glycosylated IL-7−IL-7Rα (CHO) binding interaction displays a 6900-fold faster k_1 rate than the nonglycosylated IL-7−IL-7Rα binding interaction. The glycosylated IL-7−IL-7Rα (CHO) complex has a K_d of 109 ± 15 nM, which corresponds to a $\Delta G°$ of −9.5 ± 0.1 kcal/mol, a binding enhancement of −3.3 kcal/mol versus that of the nonglycosylated IL-7−IL-7Rα complex. These values are similar to our previously published results also determined at 150 mM NaCl, pH 7.4, and 298 K (*7*).

The NaCl binding data were analyzed using an ion linkage mechanism (*14*) in which the logarithm of the equilibrium constant, K_a ($= 1/K_d$), is plotted against the negative logarithm of the NaCl concentration. The data fit best to a linear function of the form

$$\log K_a = \log K - n \log[\text{NaCl}] \quad (3)$$

where the slope indicates weaker (positive) or stronger (negative) binding with an increase in NaCl concentration. The slope, n, gives the number of sodium or chloride ions taken up or released upon formation of the complex during either the association or dissociation step. Interactions of IL-7 with nonglycosylated (●; $R^2 = 0.98$) or glycosylated (■; $R^2 = 0.97$) IL-7Rα display linear dependencies with positive slopes, indicating weaker binding affinities with increasing NaCl concentrations (Figure 3A). The nonglycosylated IL-7−IL-7Rα (EC) interaction has a slightly higher n value of 2.8 relative to a value of 2.0 for the glycosylated IL-7−IL-7Rα (CHO) interaction. The interaction of IL-7 with IL-7Rα demonstrates a strong favorable electrostatic dependence that is independent of N-linked glycosylation of IL-7Rα.

For a direct comparison to another γ_c cytokine−receptor interaction, the salt dependence of the IL-4−IL-4Rα binding interaction (▲) from a previous study by Sebald and co-workers (*15*) was plotted in Figure 3A. Of note, binding constants for binding of IL-4 to either nonglycosylated or glycosylated forms of IL-4Rα (*E. coli*, insect, or CHO cells) were similar (*15*). IL-4 also displays a linear dependence ($R^2 = 0.98$) with a weaker affinity for IL-4Rα with increasing concentrations of NaCl but has a smaller n value of 0.84 compared to that of the IL-7−IL-7Rα binding interactions. In other binding interactions of a T-cell receptor ectodomain with peptide targets, these protein−peptide interactions displayed values ranging from 0.2 to 0.4 (*16*). The binding interactions of nucleic acid binding proteins with DNA or RNA are typically characterized by strong electrostatic components with n values on the order of 2−25 ions (*14*).

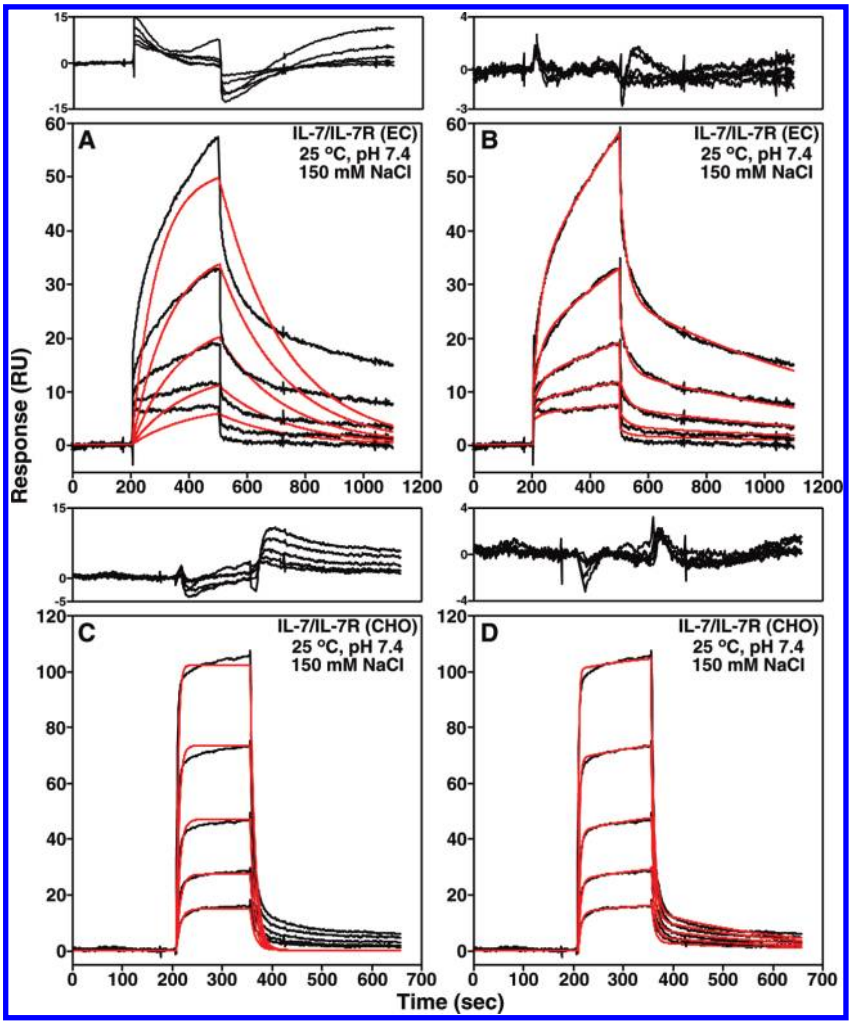

FIGURE 2: Examples of the SPR binding kinetics for binding of IL-7 to both nonglycosylated (EC) (A and B) and glycosylated (CHO) (C and D) forms of IL-7Rα in 10 mM HEPES (pH 7.4), 150 mM NaCl, 3 mM EDTA, and 0.005% Tween 20 at 298 K. The black curves are trimmed and buffer-subtracted binding sensorgrams. Twofold serial dilutions of IL-7 were performed starting at 2.5 μM for the nonglycosylated IL-7−IL-7Rα (EC) interaction and 100 nM for the glycosylated IL-7−IL-7Rα (CHO) interaction. Also displayed is the global analysis of the sensorgrams analyzed with one-step (A and C) and two-step (B and D) binding reaction models using ClampXP (*12*) and depicted as red curves. The residuals of the global fitting analysis for each binding mechanism are plotted above the sensorgrams. Note that the residual *y*-axis scales for the two-step binding reaction models are smaller in panels B and D than the residual *y*-axis scales for the one-step binding reaction models in panels A and C.

The strength of the electrostatic component of the IL-7−IL-7Rα interaction is more similar to that of a nucleic acid−protein interaction than that of a cytokine−receptor interaction.

To provide further quantitative insights into the role of electrostatics in the IL-7−IL-7Rα binding interaction, the individual rate constants were analyzed as a function of increasing NaCl concentrations from 50 mM to 1 M. Previous studies of protein−ligand interactions have demonstrated strong electrostatic components to the first kinetic k_1 on rates with an increasing ionic strength (reviewed in ref *17*). A linear dependence has been observed for the k_1 on rates with an increasing ionic strength that follows Debeye−Hückel theory using the following relationship:

$$\ln k_1 = \ln k_1^0 - \frac{U}{RT}\left(\frac{1}{1+\kappa a}\right) \quad (4)$$

where κ is the inverse of the Debeye−Hückel screening distance at a given salt concentration and a is 6 Å, the minimal distance of approach for protein−protein interactions in the transition state (*18*−*21*). The k_1^0 value defines the basal on rate in the absence of any electrostatic component. The electrostatic component of the k_1 constant is defined as $-U/RT$ at increasing salt concentrations.

A plot of ln k_1 versus $1/(1 + \kappa a)$ yields a *y*-intercept reflecting the basal k_1^0 rate constant and a slope reflecting the electrostatic energy as $-U/RT$. Figure 3B shows this plot for the IL-7−IL-7Rα and IL-4−IL-4Rα binding interactions. For IL-7 binding to nonglycosylated IL-7Rα (EC), only three data points could be analyzed because the binding kinetics and affinities are too weak above 300 mM NaCl. Poor linear regression ($R^2 = 0.11$) of these data suggests a small electrostatic component ($-U/RT$) of 0.90 ± 0.1 and a basal k_1^0 rate of $(8.6 \pm 1.2) \times 10^2$ M^{-1} s^{-1} for binding of IL-7 to nonglycosylated IL-7Rα [EC (Table 1)]. A $-U/RT$ value of 8.1 ± 0.7 and a basal k_1^0 rate of $(1.8 \pm 0.6) \times 10^4$ M^{-1} s^{-1} were obtained for binding of IL-7 to glycosylated IL-7Rα (CHO; $R^2 = 0.98$). In comparison to the IL-7−IL-7Rα (CHO) interaction, the IL-4−IL-4Rα interaction has a smaller $-U/RT$ value of 5.7 ± 0.8 but a 35-fold faster basal k_1^0 rate of $(6.3 \pm 2.7) \times 10^5$ M^{-1} s^{-1} ($R^2 = 0.94$). The electrostatic components ($-U/RT$) observed for glycosylated IL-7−IL-7Rα (CHO) and IL-4−IL-4Rα interactions fall between observed values for a TCR−A6 peptide complex [1.9 (*16*)] and the nonglycosylated erythropoietin−receptor complex [18 (*22*)].

There is a general trend of faster k_{-1} rates for IL-7 binding both the nonglycosylated and glycosylated IL-7Rα with an

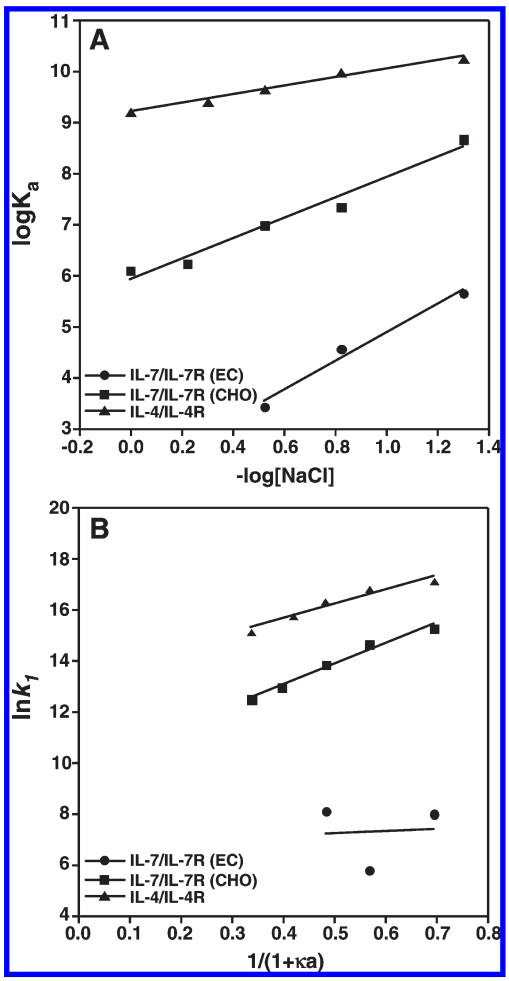

FIGURE 3: Binding interactions of IL-7 with nonglycosylated and glycosylated IL-7Rα and IL-4 with IL-4Rα as a function of salt at pH 7.4 and 298 K. The IL-4−IL-4Rα data were taken from ref *15*. (A) Equilibrium binding constants (K_a) plotted vs increasing NaCl concentrations for nonglycosylated IL-7−IL-7Rα (EC) (●), glycosylated IL-7−IL-7Rα (CHO) (■), and IL-4−IL-4Rα (▲) interactions. The data displayed a linear correlation of K_a with increasing NaCl concentrations. (B) Natural logarithm of k_1 vs NaCl concentration expressed as $1/(1 + \kappa a)$ displaying an electrostatic enhancement for the IL-7−IL-7Rα (CHO) and IL-4−IL-4Rα interactions. The data were fit using linear regression with the slopes ($-U/RT$) relating to the electrostatic energy of interaction of the first association phase (k_1) and the intercept giving the basal on rate, k_1^0. The electrostatic contributions ($-U/RT$) and k_1^0 rate constants are listed in Table 1.

Table 1: Electrostatic Contribution to the k_1 Rate Constant[a]

interaction	$-U/RT$ (kcal/mol)	k_1^0 (M^{-1} s^{-1})
IL-7−IL-7R (EC)	0.90 ± 0.1	(8.6 ± 1.2) × 10^2
IL-7−IL-7R (CHO)	8.1 ± 0.7	(1.8 ± 0.6) × 10^4
IL-4−IL-4R	5.7 ± 0.8	(6.3 ± 2.7) × 10^5

[a]Values of $-U/RT$ were obtained from the slopes of the lines from Figure 3B. Binding kinetics were measured at pH 7.4 and 298 K.

increasing ionic strength, which leads to faster dissociations of the encounter complexes (Figure S1A of the Supporting Information). For example, the k_{-1} rates for binding of IL-7 to IL-7Rα (EC) increased 3-fold as the concentration of NaCl increased from 50 to 300 mM (from 3.73 to 12.1 × 10^{-2} s^{-1}). Similarly, the k_{-1} rates increased 15-fold as the concentration of NaCl increased from 50 mM to 1 M. For the IL-4−IL-4Rα interaction, which displays single-step Langmuir binding kinetics with single k_{on} and k_{off} rate constants, the k_{off} rates do not change significantly (2-fold, 1.54 and 2.25 × 10^{-3} s^{-1}) as the concentration of NaCl increases from 50 mM to 1 M (*15*).

The second step of the binding kinetics (k_2 and k_{-2}), the transition from the encounter complex to the final IL-7−IL-7Rα complex, displays changes with increasing ionic strengths smaller than those observed for k_1 (Figure S1B,C of the Supporting Information). The k_2 rates change 2- and 9-fold for the lowest and highest NaCl concentrations for the nonglycosylated IL-7−IL-7Rα (EC) and glycosylated IL-7−IL-7Rα (CHO) complexes, respectively. The nonglycosylated IL-7−IL-7Rα (EC) complex displays faster k_{-2} rates of 3-fold as the concentration of NaCl increased from 50 to 300 mM. In contrast, the glycosylated IL-7−IL-7Rα (CHO) complex displays slower k_{-2} rates of 15-fold as the concentration of NaCl increases from 50 mM to 1 M. Thus, the data highlight a favorable long-range electrostatic contribution, primarily through the k_1 rate, to the overall binding affinity (K_d) for the interaction of IL-7 with IL-7Rα.

pH Dependence of the IL-7−IL-7Rα Interactions. Crystal structures of IL-7 bound to both nonglycosylated and glycosylated IL-7Rα revealed two histidine residues in the binding interface, which may display a pH dependence upon interaction under physiological conditions. These histidine residues are $H78^7$ of IL-7 and $H33^{7R}$ of IL-7Rα (Figure 1) (*7*). For IL-7, the side chain Nδ1 atom of $H78^7$ forms an intramolecular hydrogen bond with the side chain Oγ atom of $S19^7$ (2.9 Å) in both structures. $H78^7$ buries only 6 $Å^2$ of surface area in both complex structures. Similarly, the side chain Nδ1 atom of $H33^{7R}$ forms an intramolecular hydrogen bond to the backbone nitrogen of $E27^{7R}$ (2.9 Å) in both structures. $H33^{7R}$ also buries 5 $Å^2$ of surface area in both complex structures. The binding kinetics of IL-7 interacting with nonglycosylated and glycosylated IL-7Rα ECDs as a function of pH from pH 5.5 to 8.0 are displayed in Figure 4, and binding constants are listed individually in Tables S1 and S2 of the Supporting Information.

The largest-magnitude changes in the rate constants as a function of pH are reflected in the k_1 rates of IL-7 interacting with nonglycosylated and glycosylated IL-7Rα. There was a 294-fold faster k_1 rate going from pH 5.5 to 7.4 for the nonglycosylated IL-7−IL-7Rα (EC) interaction (0.282 × 10^2 and 83.0 × 10^2 M^{-1} s^{-1}). There was a smaller 24-fold faster change in the k_1 rate going from pH 6.0 to 7.4 for the glycosylated IL-7−IL-7Rα (CHO) interaction (0.0935 × 10^6 and 2.25 × 10^6 M^{-1} s^{-1}). The k_{-1}, k_2, and k_{-2} rates for the nonglycosylated IL-7−IL-7Rα (EC) interaction exhibited < 2-fold changes over the pH range from pH 5.5 to 8.0. The k_{-1}, k_2, and k_{-2} rates for the glycosylated IL-7−IL-7Rα (CHO) interaction exhibited 2−11-fold changes over the pH range from pH 6.0 to 8.0. The rate constants are typically faster for the glycosylated IL-7−IL-7Rα (CHO) interaction than the nonglycosylated IL-7−IL-7Rα (EC) interaction as a function of pH with the exception of the k_2 rate (Figure 4). Analysis of the pH data using a linkage mechanism as described above for the salt dependence yields linear fits from plots of log K_a versus pH with slopes of 0.86 and 0.34 for the nonglycosylated IL-7−IL-7Rα (EC; R^2 = 0.96) and glycosylated IL-7−IL-7Rα (CHO; R^2 = 0.71) interactions, respectively. These results indicate that one proton is either taken up or released when IL-7 binds to IL-7Rα, depending on the glycosylation state of the receptor. Further investigation into the pH dependence of IL-7−IL-7Rα interactions will be performed using isothermal titration calorimetry (*23*).

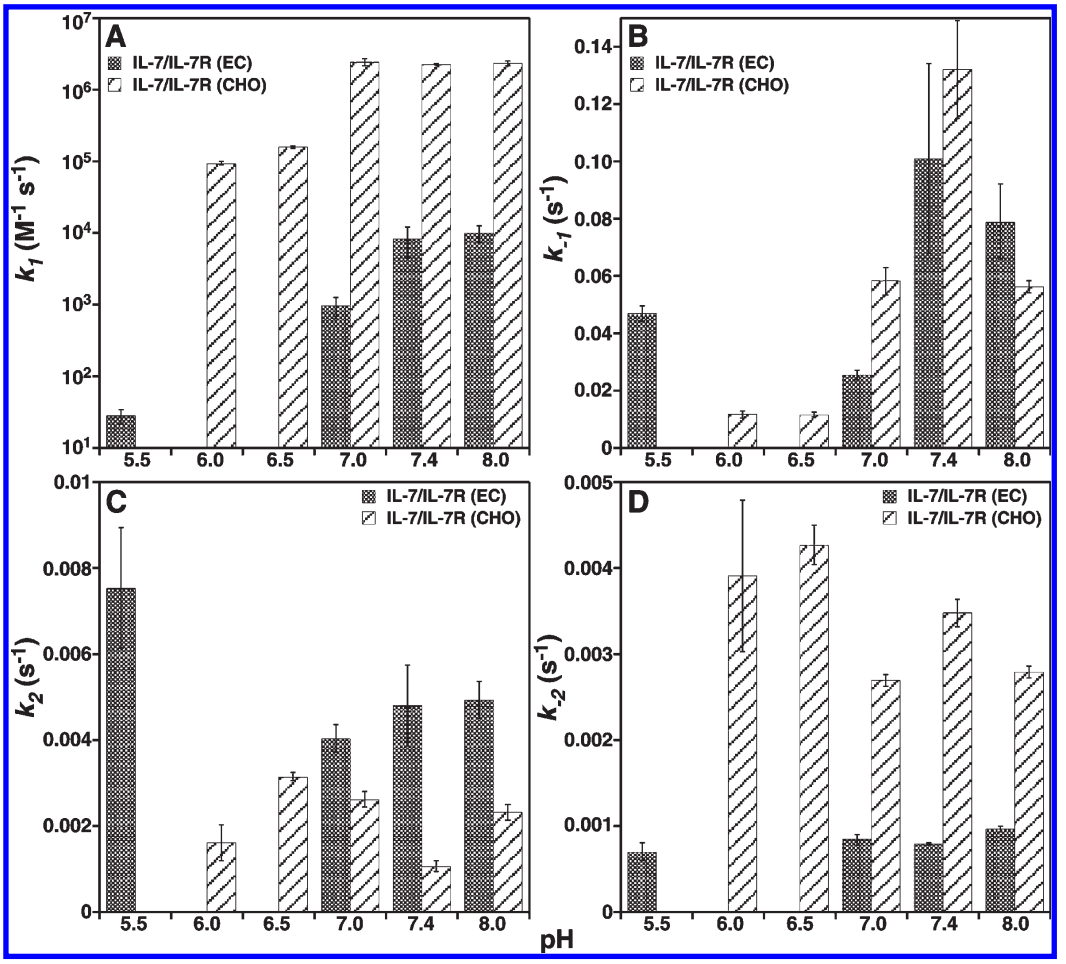

FIGURE 4: Binding kinetic constants, k_1, k_{-1}, k_2, and k_{-2}, for binding of IL-7 to nonglycosylated and glycosylated IL-7Rα as a function of pH at 150 mM NaCl and 298 K. (A) Bar graphs of k_1 constants vs pH. (B) Bar graphs of k_{-1} constants vs pH. (C) Bar graphs of k_2 constants vs pH. (D) Bar graphs of k_{-2} constants vs pH.

Equilibrium Temperature Dependence of the IL-7−IL-7Rα Binding Interactions. The SPR binding kinetics and affinities of IL-7 for nonglycosylated and glycosylated IL-7Rα were measured over a temperature range from 283 to 308 K. The individual binding constants as a function of temperature are listed in Tables S1 and S2 of the Supporting Information. The overall binding equilibrium constants (eq 2) were plotted over the temperature range using van't Hoff analysis as described by the following equation:

$$\ln K_d = \frac{\Delta H^\circ}{RT} + \frac{\Delta S^\circ}{R} \quad (5)$$

where the slope and *y*-intercept are the binding enthalpy (ΔH°) and entropy (ΔS°) changes, respectively. Figure 5A illustrates van't Hoff plots for the IL-7−IL-7Rα interactions, as well as analysis of the IL-4−IL-4Rα interaction using previously published temperature-dependent SPR binding constants (*15*). All three binding interactions fit well using linear regression, indicating that ΔH° is independent of temperature. Thus, there appears to be no or small heat capacity changes ($\Delta C_p = \Delta H^\circ/\Delta T$) upon formation of the complex that can be detected using SPR analysis (discussed in greater detail below in the Discussion).

The thermodynamic parameters governing the binding interactions of IL-7 with nonglycosylated or glycosylated IL-7Rα are defined by large favorable entropic contributions rather than enthalpic components. The nonglycosylated IL-7−IL-7Rα (EC) binding interaction has a small unfavorable enthalpy (ΔH°) change of 0.31 ± 0.09 kcal/mol and a large favorable entropy ($-T\Delta S^\circ$) change of −7.5 ± 0.2 kcal/mol (Figure 5B and Table 2). The glycosylated IL-7−IL-7Rα (CHO) binding interaction has a slightly favorable ΔH° of −0.079 ± 0.042 kcal/mol and a higher favorable $-T\Delta S^\circ$ of −9.8 ± 0.1 kcal/mol. The IL-4−IL-4Rα interaction displays a small favorable ΔH° of −0.88 ± 0.31 kcal/mol and a large favorable $-T\Delta S^\circ$ of −12.6 ± 0.7 kcal/mol.

Temperature Dependence of the IL-7−IL-7Rα Binding Kinetics. A more thorough understanding of the IL-7 binding reactions with nonglycosylated and glycosylated IL-7Rα was gained through characterization of their transition-state binding thermodynamics. The free energy changes of activation for both reaction steps were broken down into their enthalpic and entropic components using Eyring analysis as described by the following equation (*24*, *25*):

$$\ln\left(\frac{kh}{k_B T}\right) = \frac{-\Delta H^\circ}{R}\frac{1}{T} + \frac{-\Delta S^\circ}{R} \quad (6)$$

where *k* is the individual on or off rate constant (k_1, k_{-1}, k_2, or k_{-2}), *h* is Planck's constant, and k_B is Boltzmann's constant. The slope of an Eyring plot (eq 6 vs $1/T$) gives $\Delta H^{\circ\ddagger}/R$, and the *y*-intercept gives $\Delta S^{\circ\ddagger}/R$ for the individual kinetic pathway. However, it is often more accurate to calculate the entropy of activation ($\Delta S^{\circ\ddagger}$) from the relationship $\Delta G^{\circ\ddagger} = \Delta H^{\circ\ddagger} - T\Delta S^{\circ\ddagger}$ (*25*). Eyring plots of the transition-state binding thermodynamics of the IL-7−receptor interactions are provided in Figure 6, and the individual values are summarized in Table 3.

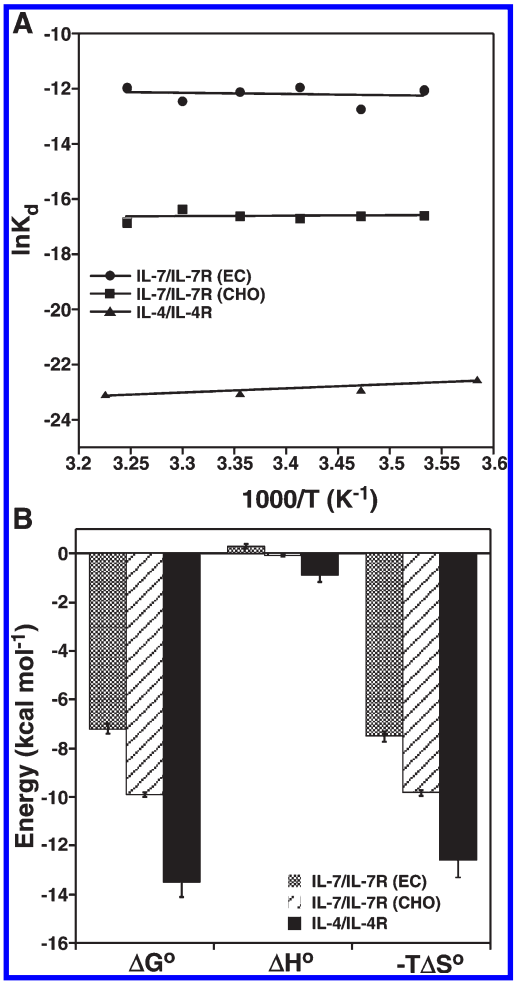

FIGURE 5: Equilibrium binding constants for binding of IL-7 to nonglycosylated and glycosylated IL-7Rα and IL-4 to IL-4Rα as a function of temperature at 150 mM NaCl and pH 7.4. (A) van't Hoff analysis plotted as ln K_d vs $1/T$ (K^{-1}). Data fit well using linear regression for nonglycosylated IL-7−IL-7Rα (EC) (●), glycosylated IL-7−IL-7Rα (CHO) (■), and IL-4−IL-4Rα (▲) interactions. (B) Bar graphs of the equilibrium thermodynamic parameters obtained from van't Hoff analysis for these interactions. These parameters are listed in Table 2. The $\Delta G°$ values are reported at 298 K.

Table 2: Equilibrium Binding Thermodynamics for IL-7 and IL-4 Interactions

interaction	$\Delta G°^a$ (kcal/mol)	$\Delta H°$ (kcal/mol)	$-T\Delta S°^b$ (kcal/mol)
IL-7−IL-7R (EC)	-7.2 ± 0.2	0.31 ± 0.09	-7.5 ± 0.2
IL-7−IL-7R (CHO)	-9.9 ± 0.1	-0.079 ± 0.042	-9.8 ± 0.1
IL-4−IL-4R	-13.5 ± 0.6^c	-0.88 ± 0.31	-12.6 ± 0.7

[a] $\Delta G°$ reported at 298 K. Experiments were performed with 150 mM NaCl at pH 7.4. [b] Calculated using the relationship $-T\Delta S° = \Delta G° - \Delta H°$. [c] Value taken from Table 2 of ref *15*.

The binding of IL-7 to nonglycosylated and glycosylated IL-7Rα exhibits differing transition-state binding thermodynamics. The Eyring plots of the binding kinetics of IL-7−IL-7Rα reactions all fit well using linear regression, indicating no measurable transition-state heat capacity changes ($\Delta C_p^{\ddagger}$) during the association or dissociation phases. As with the equilibrium ΔC_p changes described above, there may be small $\Delta C_p^{\ddagger}$ changes during the reaction pathways of the IL-7−IL-7Rα complex, but they cannot be detected in the analysis of the SPR data. During the first step in the formation of the encounter complex of IL-7 binding to IL-7Rα, the association $\Delta H°^{\ddagger}k_1$ values have opposite signs for the glycosylated and nonglycosylated IL-7Rα. The IL-7−IL-7Rα (EC) interaction has a $\Delta H°^{\ddagger}k_1$ of -15.1 ± 4.4 kcal/mol, and the IL-7−IL-7Rα (CHO) interaction has a $\Delta H°^{\ddagger}k_1$ of 8.3 ± 2.4 kcal/mol. A similar trend is observed for the dissociation $\Delta H°^{\ddagger}k_{-1}$ changes for the IL-7−IL-7Rα interactions. The IL-7−IL-7Rα (EC) interaction has a $\Delta H°^{\ddagger}k_{-1}$ of -11.1 ± 3.1 kcal/mol, and the IL-7−IL-7Rα (CHO) interaction has a $\Delta H°^{\ddagger}k_{-1}$ of 9.0 ± 1.2 kcal/mol. The second step of the reaction going from the encounter complex to the final complex displays similar transition-state enthalpies ($\Delta H°^{\ddagger}k_2$ and $\Delta H°^{\ddagger}k_{-2}$) for both the association (2.6 and 1.2 kcal/mol, respectively) and dissociation (−1.5 and −2.8 kcal/mol, respectively) of IL-7 with nonglycosylated and glycosylated IL-7Rα.

The transition-state binding entropies ($-T\Delta S°^{\ddagger}$) demonstrate the largest differences, once again, in the first step going from the unbound proteins to the encounter complexes of the IL-7−/IL-7Rα interactions. As noted previously, the transition-state entropies were calculated from the relationship $-T\Delta S°^{\ddagger} = \Delta G°^{\ddagger} - \Delta H°^{\ddagger}$ and not from the *y*-intercepts of the Eyring plots. During the association phase of the first step of the reaction, the IL-7−IL-7Rα (EC) interaction has a 38-fold higher $-T\Delta S°^{\ddagger}k_1$ (28.6 kcal/mol) than the IL-7−IL-7Rα (CHO) interaction (0.75 kcal/mol). The IL-7−IL-7Rα (EC) interaction also has a 3-fold higher $-T\Delta S°^{\ddagger}k_{-1}$ (30.8 kcal/mol) than the IL-7−IL-7Rα (CHO) interaction during the dissociation phase (9.8 kcal/mol). Similar transition-state entropies for the association and dissociation phases were observed for the second step of the reaction going from the encounter complexes to the final bound states. The $-T\Delta S°^{\ddagger}k_2$ values were 18.1 ± 1.2 and 20.5 ± 1.0 kcal/mol for the IL-7−IL-7Rα (EC) and IL-7−IL-7Rα (CHO) interactions, respectively. The $-T\Delta S°^{\ddagger}k_{-2}$ values were 23.0 ± 1.0 and 23.7 ± 0.9 kcal/mol for the IL-7−IL-7Rα (EC) and IL-7−IL-7Rα (CHO) interactions, respectively.

DISCUSSION

Electrostatics of the IL-7−IL-7Rα Interactions. This study demonstrates that electrostatics play an influential role in the interaction between IL-7 and IL-7Rα, even though the IL-7−IL-7Rα interface does not consist of multiple complementary charged residues as typically seen for electrostatically tuned protein−ligand interfaces (reviewed in ref *17*). The complex structures of IL-7 with nonglycosylated and glycosylated IL-7Rα revealed the IL-7−IL-7Rα binding interface to be the smallest (average of 740 Å^2 of buried surface area), mostly apolar in nature (47% apolar vs 33% polar residues), and least specific [four or five intermolecular hydrogen bonds with one salt bridge and an average shape complementarity (S_c) value of 0.69] relative to those of the other complex structures of γ_c family members [e.g., IL-2 and IL-4 (Figure 7)] (*7*). The IL-4−IL-4Rα binding interaction, which serves as a model system for studying favorable electrostatic steering mechanisms (reviewed in ref *17*), allows for a direct comparison with another cytokine−receptor interaction in the same family. Structural analysis of IL-4−IL-4Rα complexes (binary and ternary complexes) shows the IL-4−IL-4Rα interface buries on average 807 Å^2 of surface area (*26*, *27*). The IL-4−IL-4Rα interface consists of polar residues (43% polar vs 27% apolar) and has 14 or 15 intermolecular hydrogen bonds (depending on the complex structure analyzed) and S_c scores of 0.74 (*26*, *27*). Furthermore, numerous complementary charged residues line the IL-4−IL-4Rα interface (*26*, *27*) (Figure 7B). Glycosylation of either the IL-4 or the IL-4Rα

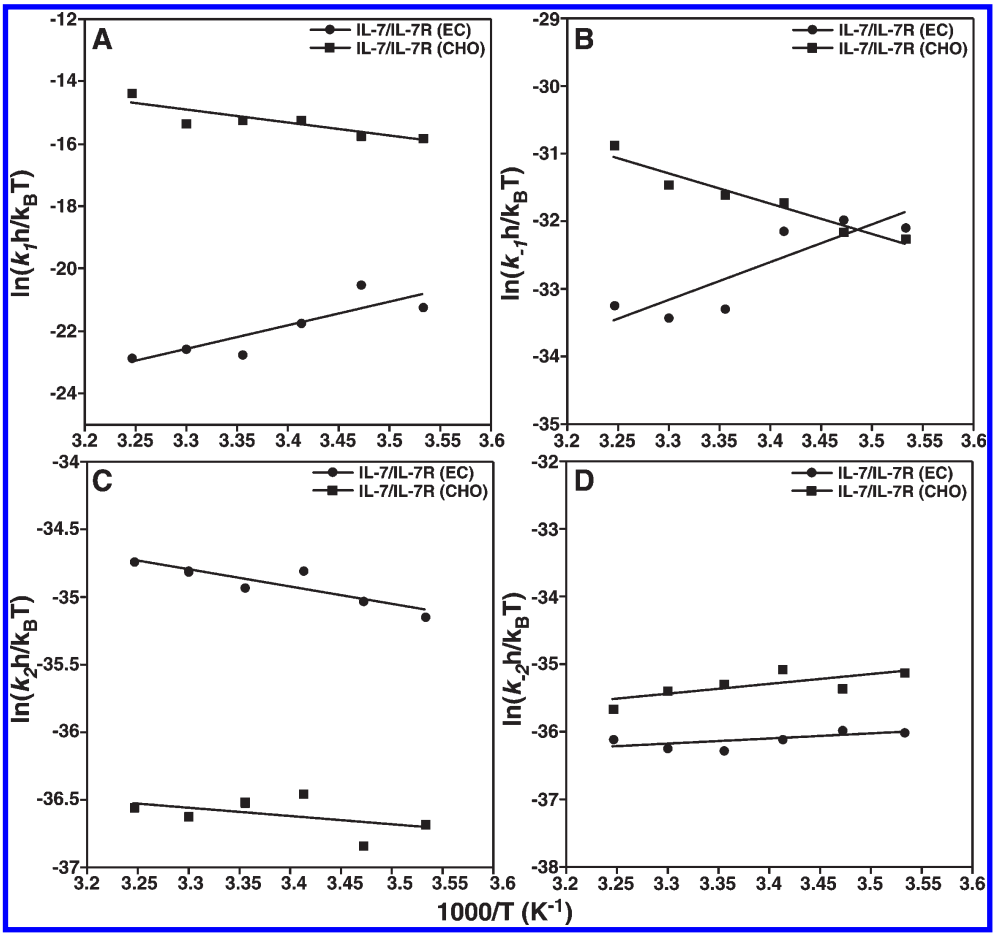

FIGURE 6: Eyring analysis of the kinetic rate constants for binding of IL-7 to nonglycosylated (●) and glycosylated (■) IL-7Rα as a function of temperature at 150 mM NaCl and pH 7.4. The data were plotted as $\ln(k_x h/k_B T)$ vs $1/T$ (K^{-1}), where k_x is an individual rate constant [k_1 (A), k_{-1} (B), k_2 (C), or k_{-2} (D)], h is Planck's constant, and k_B is Boltzmann's constant (*59*). Data fit well using linear regression. The slopes and intercepts yield transition-state enthalpies ($\Delta H^{\circ\ddagger}/R$) and entropies ($\Delta S^{\circ\ddagger}/R$) for the individual association and disassociation pathways and are listed in Table 3.

Table 3: Transition-State Binding Thermodynamics for IL-7−IL-7Rα Interactions

reaction	$\Delta G^{\circ\ddagger a}$ (kcal/mol)	$\Delta H^{\circ\ddagger}$ (kcal/mol)	$-T\Delta S^{\circ\ddagger b}$ (kcal/mol)
	First-Step k_1		
IL-7−IL-7Rα (EC)	13.5 ± 0.2	−15.1 ± 4.4	28.6 ± 2.4
IL-7−IL-7Rα (CHO)	9.04 ± 0.1	8.3 ± 2.4	0.75 ± 2.4
	First-Step k_{-1}		
IL-7−IL-7Rα (EC)	19.7 ± 0.1	−11.1 ± 3.1	30.8 ± 2.4
IL-7−IL-7Rα (CHO)	18.7 ± 0.1	9.0 ± 1.2	9.8 ± 1.2
	Second-Step k_2		
IL-7−IL-7Rα (EC)	20.7 ± 0.04	2.6 ± 0.7	18.1 ± 1.2
IL-7−IL-7Rα (CHO)	21.7 ± 0.1	1.2 ± 1.0	20.5 ± 1.0
	Second-Step k_{-2}		
IL-7−IL-7Rα (EC)	21.5 ± 0.1	−1.5 ± 0.9	23.0 ± 1.0
IL-7−IL-7Rα (CHO)	20.9 ± 0.1	−2.8 ± 1.3	23.7 ± 0.9

[a] $\Delta G^{\circ\ddagger}$ parameters at 298 K. Experiments were performed with 150 mM NaCl at pH 7.4. [b] Calculated using the relationship $-T\Delta S^{\circ\ddagger} = \Delta G^{\ddagger} - \Delta H^{\ddagger}$.

ECD does not alter their binding affinities or functional responses (*15*, *28*).

The electrostatic parameters of the IL-7−IL-7Rα binding interactions were measured by SPR responses with increasing concentrations of salt. An increased ionic strength screens electrostatic effects of binding interactions. The K_d values for binding of IL-7 to nonglycosylated and glycosylated IL-7Rα decreased with an increasing ionic strength (Figure 3A). For example, the nonglycosylated IL-7−IL-7Rα (EC) binding affinity change (ΔG° at 298 K) decreased from −7.72 to −4.68 kcal/mol as the concentration of NaCl increased from 50 to 300 mM, respectively. Above 300 mM NaCl, no binding of IL-7 to nonglycosylated IL-7Rα (EC) was detected. Similarly, the binding affinity change (ΔG° at 298 K) for binding of IL-7 to glycosylated IL-7Rα (CHO) decreased from −11.8 to −8.33 kcal/mol as the concentration of NaCl increased from 50 mM to 1 M, respectively. Analyzing the binding affinities of the IL-7−IL-7Rα interactions versus salt concentration using an ion linkage mechanism (eq 3) highlighted the fact that 2−2.8 ions are taken up or released upon formation of the complex, a number greater than the number of ions involved in ion uptake or release measured for the IL-4−IL-4Rα interaction (0.8). The ion consumption or expulsion during formation of the IL-7−IL-7Rα complex approaches that of nucleic acid binding proteins (2−25 ions), which bind negatively charged surfaces of the phosphate backbones of nucleic acids (*14*). Future studies will investigate ion linkage (salt and pH) mechanisms of the IL-7−IL-7Rα interactions using isothermal titration calorimetry (*23*).

The electrostatic attraction observed for the IL-7−IL-7Rα interactions affects the first k_1 on rate more than the other kinetic rates (k_{-1}, k_2, and k_{-2}). A linear dependence of k_1 on increasing

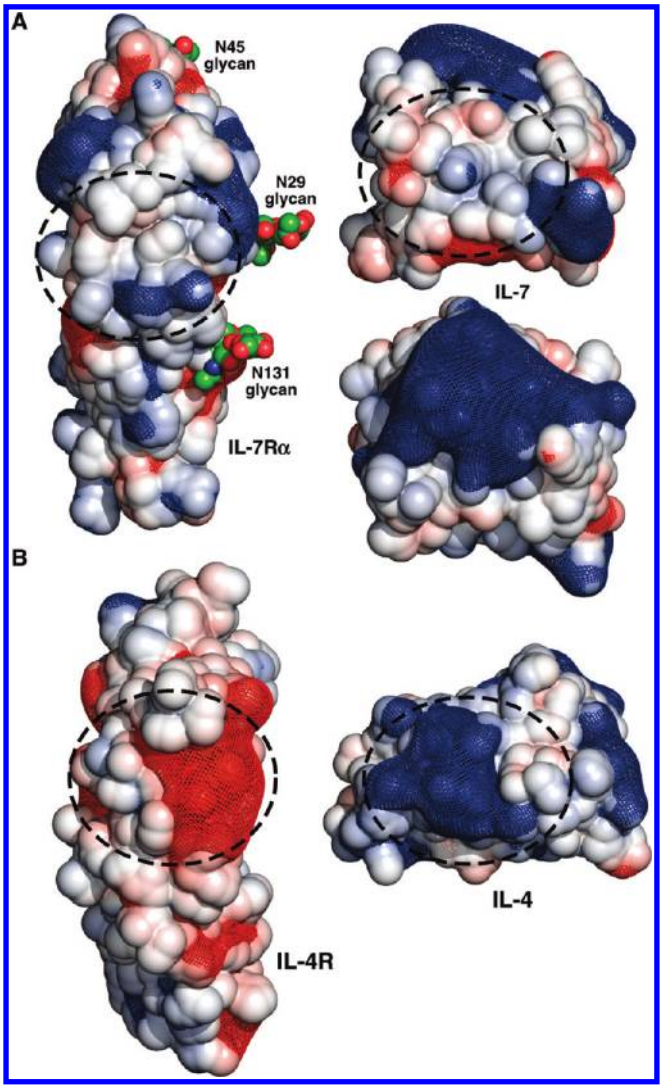

FIGURE 7: Open book view of the electrostatic surfaces and potentials for the IL-7−IL-7Rα (A) and IL-4−IL-4Rα (B) complexes. The linear Poisson−Boltzmann equation was solved for both protein complexes using APBS (*33*) with 150 mM monovalent salt at 298 K. The solvent accessible surface areas for each protein are displayed and colored blue ($5kT$/e) and red ($-5kT$/e). The electrostatic potential gradients for each protein are displayed as blue ($2kT$/e) and red ($-2kT$/e) mesh. The structures and electrostatic potentials were displayed using PyMOL (*58*). The binding interfaces for both complexes are highlighted with dashed circles. The second view of IL-7 below the view with the dashed circle is rotated 90° in the vertical direction to illustrate the large positive surface on the top of the cytokine.

NaCl concentrations was reflected in a plot of ln k_1 versus $1/(1 + \kappa a)$ following Debeye−Hückel theory (*18*) for the glycosylated IL-7−IL-7Rα (CHO) and IL-4−IL-4Rα interactions (Figure 3B). The k_1 dependence on NaCl concentration of the nonglycosylated IL-7−IL-7Rα interaction could not be reliably measured because of weakened binding constants above 300 mM NaCl. The slope of the plot of ln k_1 versus $1/(1 + \kappa a)$ gives $-U/RT$, which is the electrostatic energy enhancement. The $-U/RT$ values of 8.1 and 5.7 for the glycosylated IL-7−IL-7Rα and IL-4−IL-4Rα interactions, respectively, fall in the middle of the range observed for other protein−ligand interactions. For example, the barnase−barstar (*20*, *29*), Ifnar2−interferon α2 (*30*), TEM1−BLIP (*20*), hirudin−thrombin (*19*, *31*), heterodimeric leucine zipper (*32*), and nonglycosylated EPO−EPOR (*22*) interactions have $-U/RT$ values of 7.5, 4, 2.5−3, 13.8, 12, and 18.0, respectively. Furthermore, a protein engineering study by Schreiber and co-workers increased the $-U/RT$ electrostatic energy of the TEM1−BLIP(+6) interaction to 11−12 by introducing several surface-exposed basic residues into the BLIP protein sequence located outside of the binding interface, demonstrating the long-range nonspecific nature of electrostatics (*20*).

The contribution of electrostatics to the IL-7−IL-7Rα interactions suggests that global long-range electrostatic charges not localized at the binding interface are responsible for the observed effects. There is one salt bridge at the periphery of the IL-7−IL-7Rα binding interface between the $D74^{7}$ Oδ2 atom and the $K77^{7R}$ Nζ atom (ranging from 2.9 to 3.2 Å for the two nonglycosylated IL-7−IL-7Rα structures and one glycosylated IL-7−IL-7Rα structure) (*7*). By primary sequence analysis, IL-7 is a basic protein with an isoelectric point (pI) of 8.5 and the IL-7Rα ECD is an acidic protein with a pI of 5.4. A similar trend occurs with IL-4 (pI 9.0) and the IL-4Rα ECD (pI 5.1). Using default parameters in APBS (*33*), the linear Poisson−Boltzmann equation was solved for both IL-7−IL-7Rα and IL-4−IL-4Rα complexes at a salt concentration of 150 mM (singly charged molecules) at 298 K. The electrostatic accessible surface areas (displayed at $\pm 5kT$/e) and gradient field potentials (mesh contoured at $\pm 2kT$/e) are displayed in Figure 7 as open book views of IL-7−IL-7Rα and IL-4−IL-4Rα interfaces. Clearly, the basic charged residues of IL-4 contact the acidic charged/hydrophobic residues of IL-4Rα at the binding interface, thus providing a clear rationale for the observed electrostatic enhancement of the on rate (Figure 7B). Unlike the IL-4−IL-4Rα interface, the IL-7−IL-7Rα interface is predominately apolar in nature, and complementary electrostatic field gradients of the two binding surfaces do not drive the association (Figure 7A). The negative charge and field potential of IL-7Rα are distributed throughout the molecule and concentrated on the backside of the receptor away from the binding interface with IL-7. The positive charge and field potential of IL-7 localize to a few residues at the amino terminus and to the top part of the molecule (in Figure 7A, the IL-7 molecule is rotated 90° to highlight this feature). The concentration of basic residues on the top of IL-7 is predicted to interact with negatively charged glycosaminoglycans (GAGs), such as heparin and heparin sulfate (unpublished data). We have begun an alanine scanning study of the basic residues of IL-7 to map the binding site to GAGs. Previously, Schreiber and co-workers demonstrated that increasing the number of basic residues of BLIP that were engineered outside the TEM1−BLIP binding interface increased the binding affinity of these two proteins through faster k_{on} rates (*20*). It will be interesting to determine whether mutations of these basic residues to alanine on IL-7 for GAG interactions, which are outside the binding interface of IL-7Rα, alter the binding kinetics with IL-7Rα (especially k_1 rates).

Binding Reaction Pathways and Heat Capacity Changes of the IL-7−IL-7Rα Interactions. The interactions between IL-7 and nonglycosylated and glycosylated IL-7Rα involve binding kinetics more complex than those of previous cytokine−receptor interactions. The binding kinetics of IL-7−/IL-7Rα interactions fit best to a two-step binding reaction model in which an encounter complex is observed (Figure 2). Other cytokine−receptor interactions, especially in the γ_c family members (IL-2, IL-4, IL-15, and IL-21), fit best to a single-step reaction model with single k_{on} and k_{off} rate constants (reviewed in refs *34* and *35*). These cytokine−receptor interactions may experience encounter complexes but are transient in nature and

cannot be observed during the experimental assays. Furthermore, extensive scanning mutagenesis studies of protein−ligand interactions show the absence of electrostatic enhancement in the systems described above where k_1 on rates do not change dramatically (< 10-fold changes) (*17*, *35*). The changes in overall binding affinities ($K_d = k_{off}/k_{on}$) of various protein−protein interactions are primarily driven by changes in off rates (*17*, *35*).

The interactions of IL-7 with nonglycosylated and glycosylated forms of IL-7Rα deviate from the observed trends in protein−protein interactions and also from the behavior of γ_c family members. Of note, the trends described above have been studied for nonglycosylated protein−protein interactions or in cases where glycosylation has been determined not to be crucial to binding affinity. The 300-fold enhanced binding affinity of IL-7 for glycosylated IL-7Rα over nonglycosylated IL-7Rα results from a 4 order of magnitude faster k_1 rate change at 150 mM NaCl and 298 K with minor changes in the other three rate constants (k_{-1}, k_2, and k_{-2}). The IL-7 association mechanism changes as a function of IL-7Rα glycosylation. Specifically, the changes in the k_1 on rates switch from a "conformational" search mechanism for the nonglycosylated IL-7−IL-7Rα (EC) interaction ($k_1 = 10^2\ M^{-1}\ s^{-1}$) to a "diffusion-controlled" search mechanism for the glycosylated IL-7−IL-7Rα (CHO) interaction ($k_1 = 10^6\ M^{-1}\ s^{-1}$) (*17*). The k_1 rate of the glycosylated IL-7−IL-7Rα complex is approximately 1 order of magnitude faster than the rotational and translational diffusion limit of $10^5\ M^{-1}\ s^{-1}$ for two proteins (*17*). To the best of my knowledge, the changes in k_1 on rates as a function of the extent of IL-7Rα glycosylation are the largest reported differences for a protein−protein interaction that utilizes glycosylation for association. Previous binding studies with human granulocyte-macrophage colony stimulating factor (hGM-CSF) binding to its receptor reported a 46-fold slower k_1 on rate between nonglycosylated and glycosylated hGM-CSF (*36*). This resulted in a K_d for the hGM-CSF receptor that was weakened by 25-fold for glycosylated hGM-CSF (33 pM) versus the nonglycosylated form (820 pM) at 4 °C (*36*). In another example, EPO binding to EPOR displayed a 19-fold reduction in the k_1 on rates for binding of nonglycosylated versus glycosylated EPO to EPOR (*22*). For both hGM-CSF and EPO, glycosylation weakens the binding affinities by decelerating the k_1 on rates for their receptors. An opposite role of glycosylation is employed in the IL-7−IL-7Rα interaction, where IL-7Rα glycosylation enhances the binding affinity for IL-7 by dramatically accelerating the k_1 association.

To probe further the binding mechanisms of IL-7 interacting with nonglycosylated and glycosylated IL-7Rα, transition-state binding thermodynamics were investigated through analysis of the temperature dependence of the SPR binding kinetics. Determination of the absolute transition-state thermodynamic values from Eyring analysis of SPR biosensor kinetic data has come under considerable scrutiny (*37*, *38*). Here, I highlight the relative transition-state binding thermodynamics for the IL-7−IL-7Rα interactions because they show significant differences for the binding pathways of IL-7 and IL-7Rα with and without attached N-glycans. The reaction pathways for binding of IL-7 to both forms of IL-7Rα as a function of $\Delta G°$, $\Delta H°$, and $-T\Delta S°$ are displayed in Figure 8. The rate-determining steps of $\Delta G°$ for both binding reactions occur in the second step moving from the transition and rearrangement of the encounter complexes to the final complex states at 298 K, 150 mM NaCl, and pH 7.4. The $\Delta G°$ changes of the reaction pathways are similar for the interactions of IL-7 with nonglycosylated and glycosylated

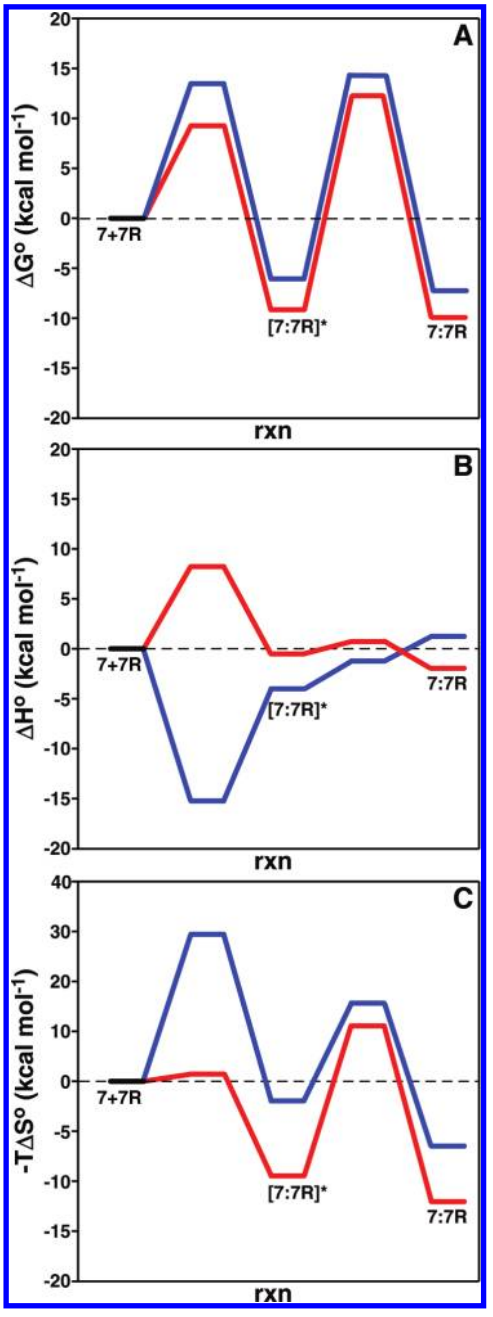

FIGURE 8: Binding reaction pathways determined from Eyring analysis for IL-7−IL-7Rα interactions for $\Delta G°$ (A), $\Delta H°$ (B), and $-T\Delta S°$ (C). The blue and red lines are for the nonglycosylated and glycosylated pathways, respectively. The transition-state thermodynamic values for the interactions are listed in Table 3.

IL-7Rα except for the first step from the unbound states to the encounter complexes ($\Delta G°^{\ddagger} k_1$ values of 13.5 and 9.04 kcal/mol). This difference between the interaction of nonglycosylated and glycosylated IL-7Rα with IL-7 at the first transition state is further propagated and not compensated by the second transition state. This accounts for the $\Delta\Delta G°$ of −3 kcal/mol (nonglycosylated minus glycosylated) for stabilization of the glycosylated IL-7−IL-7Rα pathway over the nonglycosylated IL-7−IL-7Rα pathway. The transition-state enthalpy and entropy changes further point to the first step of the two reaction pathways being responsible for the largest differences.

Differing reaction pathways are observed in the breakdown of $\Delta G°$ changes for the IL-7−IL-7Rα interactions into their transition-state enthalpies and entropies. Figure 8B displays the $\Delta H°$

reaction pathways for both interactions. The change in ΔH° from the unbound proteins to the encounter complex of the nonglycosylated IL-7−IL-7Rα (EC) interaction has a barrierless transition with a favorable $\Delta H^{\circ\ddagger}k_1$ of −15.1 kcal/mol. On the other hand, the glycosylated IL-7−IL-7Rα (CHO) complex ΔH° binding change from the unbound proteins to the encounter complex encounters an enthalpic barrier ($\Delta H^{\circ\ddagger}k_1$ of 8.3 kcal/mol) that is also the rate-determining step of the reaction coordinate. When one moves from the encounter complexes to the final states, the ΔH° changes for both IL-7−IL-7Rα interactions display comparable energies (Table 3). The overall ΔH° changes, however, for both reactions are small and have either unfavorable or favorable energies for the nonglycosylated (0.31 kcal/mol) and glycosylated (−0.079 kcal/mol) reactions. The barrierless transition of $\Delta H^{\circ\ddagger}k_1$ for the nonglycosylated IL-7−IL-7Rα interaction is rather unique: other activation enthalpies of other protein−protein systems have values similar to that of the glycosylated IL-7−IL-7Rα interaction (reviewed in ref *21*).

With regard to entropy changes ($-T\Delta S^\circ$), the rate-determining step for the IL-7−IL-7Rα binding interactions changes as a result of N-glycans attached to IL-7Rα. The rate-determining step for the nonglycosylated IL-7−IL-7Rα interaction is the first step going from the unbound proteins to the encounter complex (Figure 8C). For the glycosylated IL-7−IL-7Rα interaction, there is a $-T\Delta\Delta S^{\circ\ddagger}k_1$ (nonglycosylated minus glycosylated) change of 27.9 kcal/mol in lowering of the first step of the glycosylated IL-7−IL-7Rα pathway. This changes the rate-determining step for the glycosylated reaction to the second step going from the encounter complex to the final bound state. The magnitudes of the $-T\Delta S^{\circ\ddagger}$ changes for both IL-7−IL-7Rα reactions for the second step have similar values (Table 3). As seen with the transition-state thermodynamics of ΔG° and ΔH°, the $-T\Delta S^\circ$ data also indicate the importance of the first step going from unbound proteins to the encounter complex for the differences between the interaction of IL-7 with the IL-7Rα forms, and specifically with unbound IL-7Rα. The lowering of the $-T\Delta S^\circ$ energies from the nonglycosylated versus glycosylated pathway during the first step potentially results from the nonglycosylated IL-7Rα experiencing more conformational fluctuations than glycosylated IL-7Rα. These conformational fluctuations of nonglycosylated IL-7Rα may not allow for productive association with IL-7, whereas glycosylated IL-7Rα may restrict its structural conformations to those more conducive to interaction with IL-7. Previous studies have determined that glycosylation of proteins and peptides restrict ϕ and φ space for β-turn structures and that glycosylation stabilizes the native state (relative to the unfolded state) in the face of temperature and chemical denaturation (reviewed in ref *39*). This may offer an explanation for the differences in the k_1 rate changes observed between IL-7 and nonglycosylated IL-7Rα (EC) relative to glycosylated IL-7Rα (CHO) binding to IL-7 (10^2−10^6 M^{-1} s^{-1}). The results reported here for the IL-7−IL-7Rα interactions potentially indicate that the orientations of the two molecules are most important, rather than the specific side chain interactions, as has been demonstrated for the interactions of growth hormone and prolactin receptors (*40*). Extensive alanine scanning mutagenesis of the individual residues at the IL-7−IL-7Rα interface is underway to further answer this question.

Another unexpected finding of this study was the lack of heat capacity changes (ΔC_p) for either the equilibrium or transition states for the two IL-7−IL-7Rα interactions. The IL-7−IL-7Rα binding interface is predominately apolar in nature (47% apolar vs 33% polar residues), and one may have predicted a priori a significant negative ΔC_p from potential conformational changes of the two unbound proteins and/or desolvation of the two surfaces upon formation (*41*). Similarly, the hydrophobic transfer of solutes into water results from negative ΔC_p changes (*41*). However, both van't Hoff and Eyring analyses of the IL-7−IL-7Rα interactions showed linear dependencies as a function of temperature ($\Delta C_p = 0$). Analysis of the IL-7−IL-7Rα structures (two nonglycosylated complex structures and one glycosylated complex structure) indicates an average buried surface area of 740 Å^2 (*7*). Several research groups have parametrized the calculation of ΔC_p from the changes in accessible surface areas for apolar and polar groups at binding interfaces (*42*−*45*). Using these methods, the calculated ΔC_p values of the IL-7−IL-7Rα interface range from −238 to −413 cal mol^{-1} K^{-1}, with an average of −303 cal mol^{-1} K^{-1}. The changes in the accessible surface areas were calculated with NACCESS (*46*) using a 1.4 Å probe as described previously (*47*). A survey of experimentally determined ΔC_p values reflects an average value -80 ± 48 cal mol^{-1} K^{-1} for protein−protein interactions (*48*). The curvature induced with a ΔC_p of −303 cal mol^{-1} K^{-1} fitting to the Gibbs−Helmoltz equation would not be distinguishable from the linear regression of the van't Hoff and Eyring analysis that was performed for the IL-7−IL-7Rα interactions. Future experiments with ITC will be used to measure any ΔC_p changes for the nonglycosylated and glycosylated IL-7−IL-7Rα interactions.

Structural and Mechanistic Roles of IL-7Rα Glycosylation. The interaction between IL-7 and IL-7Rα involves a favorable electrostatic effect that is independent of the extent of IL-7Rα glycosylation. The favorable electrostatic attraction of the IL-7−IL-7Rα interaction is also not controlled by the type of N-glycan of the α-receptor, as was the case for EPO binding EPOR. In that case, removal of the negatively charged sialic acids of the three N-glycans of EPO reduced the k_{on} by 3-fold for binding to EPOR relative to fully N-glycosylated EPO (*22*). Further, the electrostatic energy ($-U/RT$) increased from 8.3 for EPO with sialic acids to 12.6 for asialo-EPO (*22*). The N-glycans of EPO do not contact the first or second binding interface of the EPORs (EPO binds to copies of EPOR) (*49*). We have previously demonstrated that the binding kinetics and affinities were similar for IL-7 and IL-7Rα produced from Schneider S2 insect cells, which produces uncharged paucimannose N-glycans, and IL-7Rα from CHO cells, which produces complex N-glycans with sialic acids (*7*). A similar electrostatic effect is likely to be seen between IL-7 and glycosylated IL-7Rα from S2 insect cells as seen in this study for the IL-7−IL-7Rα (CHO) interaction.

The attachment of N- or O-glycans to proteins may affect structure, folding−unfolding kinetics, stability, and binding−functional properties. Experiments are currently the only way to determine the extent, if any, to which glycans affect binding. Within the cytokine receptor field, N- or O-linked glycosylation of the cytokine and/or receptor typically does not alter the binding or functional (in vitro) properties of these interactions. This has been illustrated in extensive studies of the growth hormone and prolactin receptors and their hormone ligands (reviewed in ref *34*). The majority of cytokines and cytokine receptors are glycoproteins. Glycosylation is important to a few cytokines or receptors, but the effects vary in magnitude and nature. For example, N-linked glycosylation of IL-5Rα is absolutely crucial to its binding interactions with its ligands (*50*). In another example involving N-linked glycosylation of EPO, the

binding affinity is weakened for the EPOR relative to the nonglycosylated EPO (*22*). However, even with a lower binding affinity for the EPOR, glycosylated EPO displays better in vivo pharmacokinetics than the nonglycosylated counterpart (*51*).

Several general effects of glycosylation have emerged from studies of glycoproteins versus their nonglycosylated forms. Glycosylation of proteins generally increases the solubility, the stability of the native state, and the reversibility in temperature and chemical denaturations (*39*, *52*, *53*). Structurally, glycosylation of proteins may form stabilizing hydrogen bonds with surface groups, shield or reinforce hydrophobic patches on the surface of proteins, and stabilize clusters of unfavorable charged residues also on protein surfaces. Glycosylated proteins can have "chaperone" properties that enhance the overall stability of glycoproteins relative to their nonglycosylated counterparts. The attached glycans could affect the protein folding−unfolding pathways without affecting biological functions, as seen with protein chaperones (*39*, *52*, *53*). Entropic stabilization may be manifested in glycoproteins via a reduction in the level of disorder of the unfolded states of glycoproteins relative to those of their nonglycosylated proteins (*39*, *52*, *53*). A thorough study of the single N-glycan of human CD2 showed that the core trisaccharide structure of $ManGlcNAc_2$ stabilized the β-sandwich structure by 3.1 kcal/mol and accelerated the glycoprotein folding rate 4-fold versus that of the nonglycosylated form (*54*).

The structure of the glycosylated IL-7−IL-7Rα complex revealed that the N-glycans of IL-7Rα do not participate directly in the binding surface formed with IL-7 and do not induce large conformational changes in comparison to the nonglycosylated IL-7−IL-7Rα complex structure (Figure 1) (*7*). Given the biophysical data presented here, which continually point to the differences in binding constants between nonglycosylated and glycosylated IL-7Rα in the first step of the reaction pathway with IL-7, we (my research group and I) posit that structural and energetic changes induced by glycosylation of unbound IL-7Rα are being translated into enhanced allosteric binding effects for the IL-7−IL-7Rα interaction. To provide some support for this hypothesis, Figure 9 displays the far-UV CD spectra of unbound nonglycosylated (EC) and glycosylated (S2) IL-7Rα ECDs. Also displayed in Figure 9 are the far-UV CD spectra of the growth hormone receptor (hGHR) ECD. Both nonglycosylated and glycosylated IL-7Rα have peaks at 230 nm with positive ellipticity. This peak has been observed for other homology class I cytokine receptors defined by the "WSXWS" primary sequence motif in the second fibronectin type III domain (*55*−*57*). The hGHR ECD does not display the 230 nm peak presumably because it contains a "YGEFS" sequence for the WSXWS sequence motif (IL-7Rα has a "WSEWS" sequence). Glycosylated IL-7Rα (S2) has a minimum negative ellipticity peak at ∼212 nm, which is characteristic of β-sheet secondary structure (*25*). The minimum negative ellipticity peak for nonglycosylated IL-7Rα (EC) shifts from ∼212 nm in glycosylated IL-7Rα (S2) to ∼206 nm, representing an increased random coil content (*25*). The hGHR ECD, which also consists of two FNIII domains, displays a minimum negative ellipticity peak at ∼210 nm that is between the two IL-7Rα spectra. Clearly, the CD wavelength scans of nonglycosylated and glycosylated IL-7R do not overlay with each other. We hypothesize that unbound glycosylated IL-7Rα is more thermodynamically stable than unbound nonglycosylated IL-7Rα, and this enhanced stability is translated indirectly to the tighter binding to IL-7 through entropic stabilization. A further complication arises with IL-7Rα in that there are six potential N-linked glycosylation sites on the receptor: N29, N45, N131, N162, N212, and N213. Further mutagenesis and biophysical studies of the N-glycan sites of IL-7Rα will show which N-glycan(s) is/are critical to the enhanced binding constants with IL-7. In addition, structures of the nonglycosylated and glycosylated forms of unbound IL-7Rα will aid in deciphering the allosteric mechanism induced by N-linked glycosylation of the α-receptor.

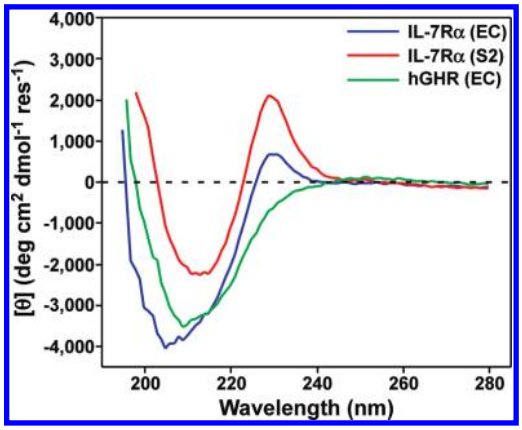

FIGURE 9: Circular dichroism spectra of unbound forms of IL-7Rαs (EC and S2) and the human growth hormone receptor (hGHR) ECDs. The spectra display the far-UV regions of nonglycosylated IL-7Rα (EC, blue), glycosylated IL-7Rα (S2, red), and hGHR (green).

ACKNOWLEDGMENT

S.T.R.W. dedicates this work to Dr. Jeff Urbauer and Mrs. Ramona Bieber Urbauer.

SUPPORTING INFORMATION AVAILABLE

Bar graphs of the k_{-1}, k_2, and k_{-2} rate constants versus increasing salt concentrations (Figure S1) and individual rate constants of the IL-7−IL-7Rα interactions for nonglycosylated (Table S1) and glycosylated (Table S2) forms. This material is available free of charge via the Internet at http://pubs.acs.org.

REFERENCES

1. Mazzucchelli, R., and Durum, S. K. (2007) Interleukin-7 receptor expression: Intelligent design. *Nat. Rev. Immunol. 7*, 144–154.
2. Rochman, Y., Spolski, R., and Leonard, W. J. (2009) New insights into the regulation of T cells by γ_c family cytokines. *Nat. Rev. Immunol. 9*, 480–490.
3. Puel, A., Ziegler, S. F., Buckley, R. H., and Leonard, W. J. (1998) Defective IL7R expression in $T^-B^+NK^+$ severe combined immunodeficiency. *Nat. Genet. 20*, 394–397.
4. Ji, R. C. (2006) Lymphatic endothelial cells, lymphangiogenesis, and extracellular matrix. *Lymphatic Res. Biol. 4*, 83–100.
5. Leonard, W. J. (2002) TSLP: Finally in the limelight. *Nat. Immunol. 3*, 605–607.
6. Goodwin, R. G., Lupton, S., Schmierer, A., Hjerrild, K. J., Jerzy, R., Clevenger, W., Gillis, S., Cosman, D., and Namen, A. E. (1989) Human interleukin 7: Molecular cloning and growth factor activity on human and murine B-lineage cells. *Proc. Natl. Acad. Sci. U.S.A. 86*, 302–306.
7. McElroy, C. A., Dohm, J. A., and Walsh, S. T. (2009) Structural and biophysical studies of the human IL-7/IL-7Rα complex. *Structure 17*, 54–65.
8. Wickham, J., Jr., and Walsh, S. T. R. (2007) Crystallization and preliminary X-ray diffraction of human interleukin-7 bound to unglycosylated and glycosylated forms of its α receptor. *Acta Crystallogr. F63*, 865–869.
9. Walsh, S. T., Jevitts, L. M., Sylvester, J. E., and Kossiakoff, A. A. (2003) Site2 binding energetics of the regulatory step of growth hormone-induced receptor homodimerization. *Protein Sci. 12*, 1960–1970.
10. Walsh, S. T., Sylvester, J. E., and Kossiakoff, A. A. (2004) The high- and low-affinity receptor binding sites of growth hormone are allosterically coupled. *Proc. Natl. Acad. Sci. U.S.A. 101*, 17078–17083.

11. Morton, T. A., Myszka, D. G., and Chaiken, I. M. (1995) Interpreting complex binding kinetics from optical biosensors: A comparison of analysis by linearization, the integrated rate equation, and numerical integration. *Anal. Biochem. 227*, 176–185.
12. Myszka, D. G., and Morton, T. A. (1998) Clamp: A biosensor kinetic data analysis program. *Trends Biochem. Sci. 23*, 149–150.
13. Bevington, P. R., and Robinson, D. K. (2003) Data Reduction and Error Analysis for the Physical Sciences, 3rd ed., McGraw-Hill, Burr Ridge, IL.
14. Record, M. T., Jr., Anderson, C. F., and Lohman, T. M. (1978) Thermodynamic analysis of ion effects on the binding and conformational equilibria of proteins and nucleic acids: The roles of ion association or release, screening, and ion effects on water activity. *Q. Rev. Biophys. 11*, 103–178.
15. Shen, B. J., Hage, T., and Sebald, W. (1996) Global and local determinants for the kinetics of interleukin-4/interleukin-4 receptor α chain interaction. A biosensor study employing recombinant interleukin-4-binding protein. *Eur. J. Biochem. 240*, 252–261.
16. Davis-Harrison, R. L., Armstrong, K. M., and Baker, B. M. (2005) Two different T cell receptors use different thermodynamic strategies to recognize the same peptide/MHC ligand. *J. Mol. Biol. 346*, 533–550.
17. Schreiber, G., Haran, G., and Zhou, H. X. (2009) Fundamental Aspects of Protein-Protein Association Kinetics. *Chem. Rev. 109*, 839–860.
18. Vijayakumar, M., Wong, K. Y., Schreiber, G., Fersht, A. R., Szabo, A., and Zhou, H. X. (1998) Electrostatic enhancement of diffusion-controlled protein-protein association: Comparison of theory and experiment on barnase and barstar. *J. Mol. Biol. 278*, 1015–1024.
19. Selzer, T., and Schreiber, G. (1999) Predicting the rate enhancement of protein complex formation from the electrostatic energy of interaction. *J. Mol. Biol. 287*, 409–419.
20. Selzer, T., Albeck, S., and Schreiber, G. (2000) Rational design of faster associating and tighter binding protein complexes. *Nat. Struct. Biol. 7*, 537–541.
21. Schreiber, G. (2002) Kinetic studies of protein-protein interactions. *Curr. Opin. Struct. Biol. 12*, 41–47.
22. Darling, R. J., Kuchibhotla, U., Glaesner, W., Micanovic, R., Witcher, D. R., and Beals, J. M. (2002) Glycosylation of erythropoietin affects receptor binding kinetics: Role of electrostatic interactions. *Biochemistry 41*, 14524–14531.
23. Baker, B. M., and Murphy, K. P. (1996) Evaluation of linked protonation effects in protein binding reactions using isothermal titration calorimetry. *Biophys. J. 71*, 2049–2055.
24. Eyring, H. (1935) The activated complex and the absolute rate of chemical reactions. *Chem. Rev. 17*, 65–77.
25. Fersht, A. (1999) Stucture and mechanism in protein science, W. H. Freeman and Co., New York.
26. Hage, T., Sebald, W., and Reinemer, P. (1999) Crystal structure of the interleukin-4/receptor α chain complex reveals a mosaic binding interface. *Cell 97*, 271–281.
27. Laporte, S. L., Juo, Z. S., Vaclavikova, J., Colf, L. A., Qi, X., Heller, N. M., Keegan, A. D., and Garcia, K. C. (2008) Molecular and Structural Basis of Cytokine Receptor Pleiotropy in the Interleukin-4/13 System. *Cell 132*, 259–272.
28. Reinemer, P., Sebald, W., and Duschl, A. (2000) The Interleukin-4-Receptor: From Recognition Mechanism to Pharmacological Target Structure. *Angew. Chem., Int. Ed. 39*, 2834–2846.
29. Schreiber, G., and Fersht, A. R. (1996) Rapid, electrostatically assisted association of proteins. *Nat. Struct. Biol. 3*, 427–431.
30. Piehler, J., and Schreiber, G. (1999) Biophysical analysis of the interaction of human ifnar2 expressed in *E. coli* with IFNα2. *J. Mol. Biol. 289*, 57–67.
31. Stone, S. R., Dennis, S., and Hofsteenge, J. (1989) Quantitative evaluation of the contribution of ionic interactions to the formation of the thrombin-hirudin complex. *Biochemistry 28*, 6857–6863.
32. Wendt, H., Leder, L., Harma, H., Jelesarov, I., Baici, A., and Bosshard, H. R. (1997) Very rapid, ionic strength-dependent association and folding of a heterodimeric leucine zipper. *Biochemistry 36*, 204–213.
33. Baker, N. A., Sept, D., Joseph, S., Holst, M. J., and McCammon, J. A. (2001) Electrostatics of nanosystems: Application to microtubules and the ribosome. *Proc. Natl. Acad. Sci. U.S.A. 98*, 10037–10041.
34. Kossiakoff, A. A. (2004) The structural basis for biological signaling, regulation, and specificity in the growth hormone-prolactin system of hormones and receptors. *Adv. Protein Chem. 68*, 147–169.
35. Kossiakoff, A. A., and Koide, S. (2008) Understanding mechanisms governing protein-protein interactions from synthetic binding interfaces. *Curr. Opin. Struct. Biol. 18*, 499–506.
36. Cebon, J., Nicola, N., Ward, M., Gardner, I., Dempsey, P., Layton, J., Duhrsen, U., Burgess, A. W., Nice, E., and Morstyn, G. (1990) Granulocyte-macrophage colony stimulating factor from human lymphocytes. The effect of glycosylation on receptor binding and biological activity. *J. Biol. Chem. 265*, 4483–4491.
37. Winzor, D. J., and Jackson, C. M. (2005) Interpretation of the temperature dependence of rate constants in biosensor studies. *Anal. Biochem. 337*, 289–293.
38. Winzor, D. J., and Jackson, C. M. (2006) Interpretation of the temperature dependence of equilibrium and rate constants. *J. Mol. Recognit. 19*, 389–407.
39. Mitra, N., Sinha, S., Ramya, T. N., and Surolia, A. (2006) N-Linked oligosaccharides as outfitters for glycoprotein folding, form and function. *Trends Biochem. Sci. 31*, 156–163.
40. Horn, J. R., Sosnick, T. R., and Kossiakoff, A. A. (2009) Principal determinants leading to transition state formation of a protein-protein complex, orientation trumps side-chain interactions. *Proc. Natl. Acad. Sci. U.S.A. 106*, 2559–2564.
41. Chandler, D. (2005) Interfaces and the driving force of hydrophobic assembly. *Nature 437*, 640–647.
42. Murphy, K. P., and Freire, E. (1992) Thermodynamics of structural stability and cooperative folding behavior in proteins. *Adv. Protein Chem. 43*, 313–361.
43. Spolar, R. S., and Record, M. T., Jr. (1994) Coupling of local folding to site-specific binding of proteins to DNA. *Science 263*, 777–784.
44. Makhatadze, G. I., and Privalov, P. L. (1995) Energetics of protein structure. *Adv. Protein Chem. 47*, 307–425.
45. Myers, J. K., Pace, C. N., and Scholtz, J. M. (1995) Denaturant m values and heat capacity changes: Relation to changes in accessible surface areas of protein unfolding. *Protein Sci. 4*, 2138–2148.
46. Hubbard, S., and Thornton, J. (1993) NACCESS, Department of Biochemistry and Molecular Biology, University College London, London.
47. Baker, B. M., and Murphy, K. P. (1998) Prediction of binding energetics from structure using empirical parameterization. *Methods Enzymol. 295*, 294–315.
48. Stites, W. E. (1997) Protein-protein interactions: Interface structure, binding thermodynamics, and mutational analysis. *Chem. Rev. 97*, 1233–1250.
49. Syed, R. S., Reid, S. W., Li, C., Cheetham, J. C., Aoki, K. H., Liu, B., Zhan, H., Osslund, T. D., Chirino, A. J., Zhang, J., Finer-Moore, J., Elliott, S., Sitney, K., Katz, B. A., Matthews, D. J., Wendoloski, J. J., Egrie, J., and Stroud, R. M. (1998) Efficiency of signalling through cytokine receptors depends critically on receptor orientation. *Nature 395*, 511–516.
50. Johanson, K., Appelbaum, E., Doyle, M., Hensley, P., Zhao, B., Abdel-Meguid, S. S., Young, P., Cook, R., Carr, S., and Matico, R.; et al. (1995) Binding interactions of human interleukin 5 with its receptor α subunit. Large scale production, structural, and functional studies of *Drosophila*-expressed recombinant proteins. *J. Biol. Chem. 270*, 9459–9471.
51. Egrie, J. C., and Browne, J. K. (2001) Development and characterization of novel erythropoiesis stimulating protein (NESP). *Br. J. Cancer 84* (Suppl. 1), 3–10.
52. Dwek, R. A. (1996) Glycobiology: Toward Understanding the Function of Sugars. *Chem. Rev. 96*, 683–720.
53. Wyss, D. F., and Wagner, G. (1996) The structural role of sugars in glycoproteins. *Curr. Opin. Biotechnol. 7*, 409–416.
54. Hanson, S. R., Culyba, E. K., Hsu, T. L., Wong, C. H., Kelly, J. W., and Powers, E. T. (2009) The core trisaccharide of an N-linked glycoprotein intrinsically accelerates folding and enhances stability. *Proc. Natl. Acad. Sci. U.S.A. 106*, 3131–3136.
55. Anaguchi, H., Hiraoka, O., Yamasaki, K., Naito, S., and Ota, Y. (1995) Ligand binding characteristics of the carboxyl-terminal domain of the cytokine receptor homologous region of the granulocyte colony-stimulating factor receptor. *J. Biol. Chem. 270*, 27845–27851.
56. Ozbek, S., Grotzinger, J., Krebs, B., Fischer, M., Wollmer, A., Jostock, T., Mullberg, J., and Rose-John, S. (1998) The membrane proximal cytokine receptor domain of the human interleukin-6 receptor is sufficient for ligand binding but not for gp130 association. *J. Biol. Chem. 273*, 21374–21379.
57. Hensley, P., Doyle, M. L., Myszka, D. G., Woody, R. W., Brigham-Burke, M. R., Erickson-Miller, C. L., Griffin, C. A., Jones, C. S., McNulty, D. E., O'Brien, S. P., Amegadzie, B. Y., MacKenzie, L., Ryan, M. D., and Young, P. R. (2000) Evaluating energetics of erythropoietin ligand binding to homodimerized receptor extracellular domains. *Methods Enzymol. 323*, 177–207.
58. DeLano, W. (2002) The PyMOL Molecular Graphics System, DeLano Scientific, San Carlos, CA.
59. Roos, H., Karlsson, R., Nilshans, H., and Persson, A. (1998) Thermodynamic analysis of protein interactions with biosensor technology. *J. Mol. Recognit. 11*, 204–210.